Instability of a contact surface driven by a nonuniform shock wave

R. Ishizaki,[1] K. Nishihara,[1] H. Sakagami,[2] and Y. Ueshima[1]
[1]*Institute of Laser Engineering, Osaka University, Suita, Osaka 565 Japan*
[2]*Himeji Institute of Technology, Himeji, Hyogo 671-22 Japan*
(Received 18 October 1995; revised manuscript received 18 March 1996)

Stability of a uniform contact surface is investigated in the case when a nonuniform shock wave passes through the surface. The nonuniform shock is generated by a rippled piston that moves with constant velocity. The amplitude of the shock oscillates and decreases as it propagates. A uniform contact surface is found to be unstable after the nonuniform shock passes across it. The growth rate depends sensitively on the phase of the oscillating shock wave at the time when the shock hits the contact surface. The physical mechanism of the instability is qualitatively discussed. The linear and nonlinear evolutions of the instability are studied. In particular, the dependence of the linear case on the Atwood number for a weak shock is investigated. Properties of this stability are found to exhibit differences from those of the standard Richtmyer-Meshkov instability in both the linear and nonlinear cases. [S1063-651X(96)50406-X]

PACS number(s): 52.35.−g

In inertial confinement fusion, fuel is required to be compressed approximately up to 1000 times solid density. An asymmetric implosion associated with hydrodynamic instabilities disturbs uniform high density compression and reduces fusion reaction yield. Nonuniform laser irradiation leads to nonuniform ablation and thus to the generation of nonuniform shock waves. This could seed density perturbations that will grow later due to the Rayleigh-Taylor (RT) instability in the acceleration phase. This happens even if the target surface is initially uniform.

It is well known that a nonuniform contact surface becomes unstable when a (uniform) shock wave passes through the contact surface because of the so-called Richtmyer-Meshkov (RM) instability [1,2]. In this paper we investigate the stability of a uniform contact surface when the nonuniform shock passes through it. It will be shown that the uniform contact surface becomes unstable and the growth rate depends on the phase of the oscillating shock wave at the time when the shock hits the material interface. Both linear and nonlinear evolutions of the instability are found to have differences from the RM instability.

We consider a shock wave driven by a rippled piston as shown in Fig. 1(a). In the figure, the piston is located at $z=0$ in a reference frame moving with the piston, and the shock propagates in the z direction with the speed of v_s relatively to the piston. We consider the surface modulation of the piston to be given as $a_0\exp(ikx)$, where a_0 and k are the amplitude and the wave number, respectively. The surface modulation of the piston induces perturbations of velocity u, density ρ, and pressure p in the shock compressed region.

In the linear theory [1], the pressure perturbation in the shock compressed region satisfies the wave equation:

$$\frac{\partial^2 p_1^1(z,t)}{\partial t^2}=c_1^{0^2}\frac{\partial^2 p_1^1(z,t)}{\partial z^2}-c_1^{0^2}k^2 p_1^1(z,t), \tag{1}$$

where c_1 is the sound speed in the shock compressed region. The subscripts 0, 1, and 2 denote, respectively, the values ahead of the shock, behind the shock, and beyond the contact surface as shown in Fig. 1(a). The superscripts 0 and 1 denote the unperturbed and first-order quantities, respectively. The pressure perturbation in the compressed region perturbs the shock speed which is equal to the time derivative of the shock surface ripple. From the shock Hugoniot condition, the amplitude of the shock surface ripple [1], $a_s(t)$, is thus given by

$$\dot{a}_s(t)=\frac{\gamma+1}{4\rho_0^0 c_0^0 M}p_1^1(v_s t,t), \tag{2}$$

where M is the shock Mach number and γ is the isentropic exponent.

To solve Eq. (1) we make a linear perturbation of the Hugoniot relationship at the shock front and use the fact that no perturbation exists ahead of the front and that the tangential velocity is continuous at both sides of the shock. Thus, we obtain, following Ref. [1],

$$\frac{1}{c_0^0}\left[\frac{M}{2\gamma M^2-(\gamma-1)}+\frac{M^2+1}{2M\{(\gamma-1)M^2+2\}}\right]\frac{dp_1^1(v_s t,t)}{dt}+\frac{M^2-1}{2\gamma M^2-(\gamma-1)}\left[\frac{\partial p_1^1(z,t)}{\partial z}\right]_{z=v_s t}+2k^2\rho_0^0 c_0^{0^2}\frac{(M^2-1)}{(\gamma+1)}a_s(t)=0. \tag{3}$$

At the piston, we have $\partial p_1^1(0,t)/\partial z=0$. The initial conditions are given by $a_s(0)=a_0$ and $p_1^1(0,0)=0$.

We can solve Eq. (1) in the domain $t\geqslant 0$, $0\leqslant z\leqslant v_s t$. Figure 2 shows the amplitude of the rippled shock surface, $a_s(t)$, as a function of the normalized time, $v_s t/\lambda$, where λ is the wavelength of the perturbation ($\lambda=2\pi/k$). The parameters used are $p_0=1$ Mbar, $\rho_0=0.01$ g/cm^3, $M=2$, $a_0/\lambda=0.01$, and $\lambda=100$ μm. Open circles show simulation results obtained by using the two-dimensional fluid code IMPACT-2D [3], in which fully Eulerian and Cartesian coordinate systems are employed, and the basic conservation equations for mass, momentum, and total energy density are numerically solved with an explicit total variation diminishing scheme [4]. Solid line is the theoretical value obtained from Eqs. (1)–(3). They are seen in good agreement. It is clearly

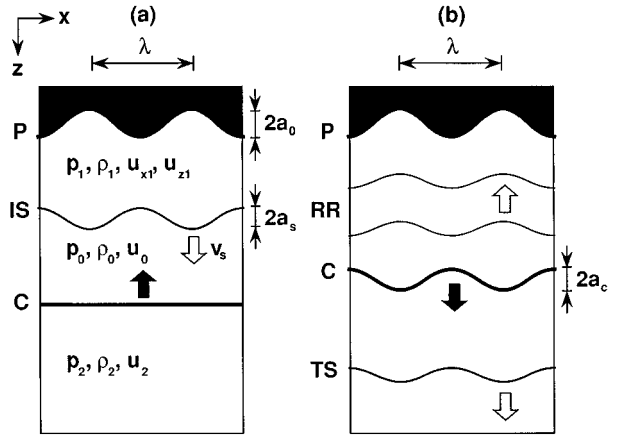

FIG. 1. Illustration of a nonuniform shock driven by a rippled piston at a few time steps (a) prior to and (b) after the shock passes a uniform contact surface in a reference frame moving with the piston. *P* and *C* denote the piston and contact surface. IS and TS are the incident and transmitted shock waves, and RR the reflected rarefaction wave for the case of $\rho_0 > \rho_2$. $\rho_0 = 0.01$ g/cm^3, $\rho_1 = 16\rho_0/7$, and $\rho_2 = \rho_0/3$.

seen that the rippled shock front oscillates and decays as it propagates [5]. The oscillating amplitude of the rippled shock surface decays asymptotically as $t^{-3/2}$ for weak shocks ($t^{-1/2}$ for strong shocks) as it propagates out from the piston [6]. The decay was also observed in experiments [7]. It should also be noted that when the perturbation amplitude of the rippled shock is zero (for example, the phases 1 and 3 in Fig. 2), the perturbations of the longitudinal velocity, u_{z1}^1, pressure, p_1^1, and density, ρ_1^1, have their maximum values at the shock front ($z = v_s t$). On the other hand, when the perturbation amplitude is maximum (for example, the phase 2 in Fig. 2), the transverse velocity perturbation, u_{x1}^1, has its maximum value and the other perturbations become zero.

Next, we consider that the nonuniform shock wave propagates through a uniform contact surface. We show the rippled piston, rippled shock and contact surface at a few time steps prior to and after shock passes the uniform contact surface in Figs. 1(a) and 1(b), respectively. In the case that

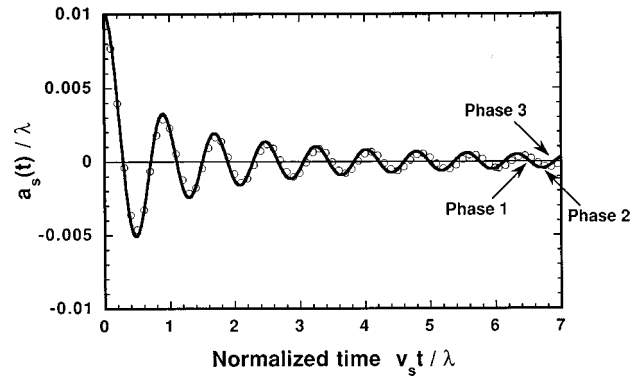

FIG. 2. Normalized amplitude of the rippled shock surface, $a_s(t)/\lambda$, as a function of the normalized time, $v_s t/\lambda$. Solid line is the theoretical value obtained from Eq. (1). Open circles show simulation results. Phases 1 and 3 correspond to the time when the amplitude of the rippled shock surface becomes zero and phase 2 the time when the amplitude has a maximum value.

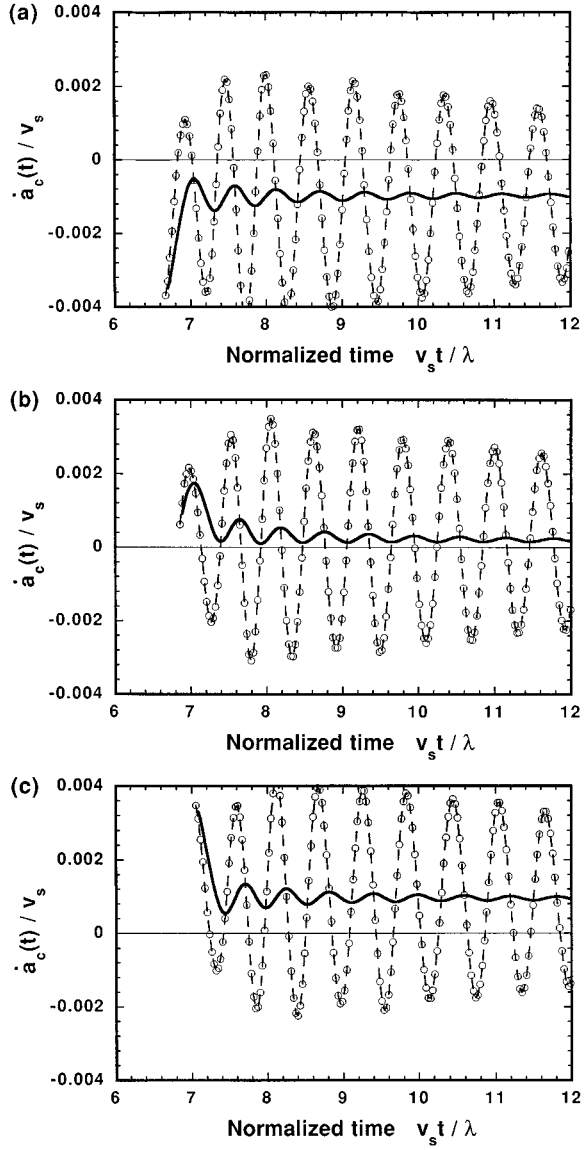

FIG. 3. Normalized growth rate (velocity perturbation) of the unstable contact surface, $\dot{a}_c(t)/v_s$, as functions of the normalized time, $v_s t/\lambda$. Open circles (dashed line) are simulation results and the solid line is the time averaged value, $\langle \dot{a}_c(t)/v_s \rangle$. (a), (b), and (c) correspond to the cases where the rippled shock hits the uniform contact surface at phases 1, 2, and 3 in Fig. 2, respectively.

the shock propagates through the contact surface from the high density fluid (ρ_0) to the low density fluid (ρ_2), the reflected rarefaction (RR) and transmitted shock (TS) propagate in the compression region (ρ_1) and the low density region (ρ_2), respectively, after the shock hits the contact surface. We first discuss the linear growth of the contact surface. The growth rates of the contact surface perturbation induced by the propagation of the nonuniform shock wave are examined for three different cases. Namely, the shock hits the contact surface at the three different oscillating phases of the shock corresponding to the phases 1, 2, and 3 around the normalized time $v_s t/\lambda = 6 \sim 7$ in Fig. 2. The normalized velocity perturbations of the contact surface, $\dot{a}_c(t)/v_s$, are shown as open circles in Figs. 3(a), 3(b), and 3(c) corresponding to the phases 1, 2, and 3 in Fig. 2, respectively, where $a_c(t)$ is the perturbation amplitude of the contact surface. The Atwood number of the contact surface,

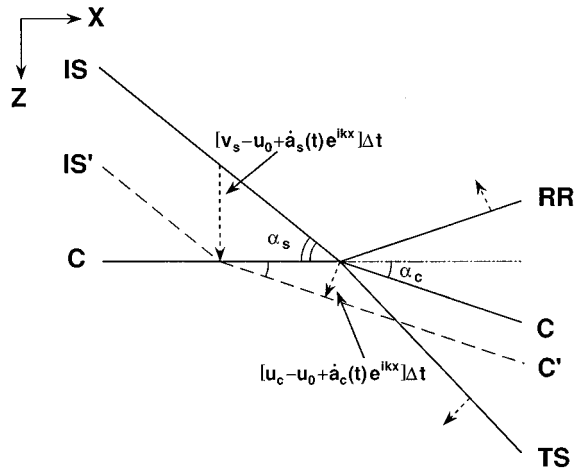

FIG. 4. Schematic drawing of an oblique shock perturbation through a contact surface for a negative Atwood number, $A<0$. IS, TS, RR, and C are the same as in Fig. 1. IS′ and C' are the incident shock and contact surface after a time Δt.

$A=(\rho_2-\rho_0)/(\rho_2+\rho_0)$, is equal to -0.5 and therefore a rarefaction is reflected. For all these cases the velocity perturbations of the contact surface oscillate with the same period and phase as the velocity perturbation behind the shock. However, their time averaged values, $\langle \dot{a}_c(t)\rangle/v_s$, are different for the three cases. We define $\langle \dot{a}_c(t)\rangle = \int_{t_0}^{t} \dot{a}_c(t')dt'/(t-t_0)$, where t_0 is the time when the shock hits the contact surface. They are indicated by the solid lines in Fig. 3. The averaged perturbation velocity of the contact surface, $\langle \dot{a}_c(t)\rangle$, is negative for the phase 1, $\langle \dot{a}_c(t)\rangle \approx 0$ for the phase 2, and $\langle \dot{a}_c(t)\rangle$ is positive for the phase 3. The perturbation velocity of the contact surface is in phase with the shock ripple perturbation velocity at the moment the shock crosses the contact surface. The growth rates of the instability driven by the nonuniform shock thus depend on the phase of the oscillating shock at the time when the shock hits the contact surface. The dependence of the growth rates on the shock phase is found to be similar even for different Atwood numbers as will be shown later.

The physical mechanism of the instability and the strong dependence of the growth rate on the phase of the oscillating shock can be understood as follows. When the rippled shock hits the uniform contact surface, the shock induces the velocity perturbation of the contact surface, impulsively. The velocity perturbation of the contact surface can be estimated by considering that an oblique shock hits the contact surface. As shown in Fig. 4, in a time of Δt, the incident shock moves a distance of $[v_s-u_0+\dot{a}_x(t)e^{ikx}]\Delta t$ in the z direction, in the laboratory frame, while the intersection of the incident shock and the contact surface moves a distance of $[v_s-u_0+\dot{a}_s(t)e^{ikx}]\Delta t/\tan\alpha_s$ along the contact surface. Therefore, the contact surface moves a distance $[v_s-u_0+\dot{a}_s(t)e^{ikx}]\Delta t \sin\alpha_c/\tan\alpha_s$ normal to itself. Since the contact surface velocity is $u_c-u_0+\dot{a}_c(t)e^{ikx}$ in the laboratory frame, we have

$$u_c-u_0+\dot{a}_c(t)e^{ikx}=[v_s-u_0+\dot{a}_s(t)e^{ikx}]\frac{\sin\alpha_c}{\tan\alpha_s}. \quad (4)$$

For small angles, $\sin\alpha\approx\tan\alpha\approx\alpha$, and we obtain $\alpha_c:\alpha_s=u_c-u_0:v_s-u_0$ from the zeroth-order terms of Eq. (4). We then obtain the velocity perturbation of the contact surface induced by the impact of the rippled shock front from the first-order terms, in the form

$$\dot{a}_c(t_0)=\frac{u_c-u_0}{v_s-u_0}\dot{a}_s(t_0). \quad (5)$$

The pressure perturbation behind the rippled shock is a damped oscillation. For simplicity we assume that the contact surface is accelerated continuously, in the form, $g(t)=\Delta g \exp\{-\Gamma(t-t_0)\rangle\sin\{\omega(t-t_0)+\phi\}$, where ϕ is the phase of the oscillating shock at the time t_0, and Δg is a constant value. ω and Γ are the oscillating frequency and damping rate of the acceleration, and they are assumed to be constants. The growth rate of the instability is estimated by integrating the acceleration, $\dot{a}_c(t)=\dot{a}_c(t_0)-\int_{t_0}^{t} g(t)dt$.

Now we make $t\to\infty$ and assume $\omega\gg\Gamma$, thus getting

$$\langle\langle \dot{a}_c\rangle\rangle=\dot{a}_c(t_0)-\frac{\Delta g}{\omega}\cos\phi, \quad (6)$$

where $\langle\langle\ \rangle\rangle$ expressed an asymptotic value, $\ll\dot{a}_c\gg = \lim_{t\to\infty}\langle \dot{a}_c(t)\rangle = \lim_{t\to\infty}\dot{a}_c(t)$.

Equation (6) clearly indicates that the growth rate depends on the phase of the oscillating shock at the time when the shock hits the contact surface. It can also be shown that the growth rate depends on the phase in the case that the acceleration decays proportionally to t^{-n} $(n<0)$.

We show the explicit dependence of $\langle\langle \dot{a}_c\rangle\rangle$ on the phase of $\dot{a}_s$ at $t=t_0$. The longitudinal gravity perturbation is $g(t)\sim[\partial p^1/\partial z]_{z=z_c}$, where z_c is the position of the contact surface. From Eq. (2) we see that $\dot{p}_1^1(v_s t,t)$ has the same phase as $\ddot{a}_s(t)$. Then from Eq. (3) we deduce that $g(t_0)$ has the same phase as $a_s(t_0)$. Namely, we obtain $a_c(t_0)\propto a_s(t_0)\propto\cos\phi$. Thus the first and the second terms in Eq. (6) have the same phase. If in Eq. (6) we assume that the second term is proportional to the first one, then it results that

$$\langle\langle \dot{a}_c\rangle\rangle=D\frac{u_c-u_0}{v_s-u_0}\dot{a}_s(t_0), \quad (7)$$

where D is a constant value. The validity of Eq. (7) will be shown later for various Atwood numbers. Equation (7) indicates clearly that the growth rate depends on the phase of the oscillating shock at the time when the shock hits the contact surface. The instability can thus be understood as a gravitational instability where the acceleration is induced by the velocity perturbation of the shock front and by the oscillatory damped pressure perturbation behind it.

The dependence of the growth rate on the Atwood number is investigated for three different phases of the shock. The results are shown in Fig. 5, where open circles, squares, and triangles correspond to the phases 1, 2, and 3 in Fig. 2, respectively. The solid, dotted, and dot-dashed lines express the theoretical values obtained from Eq. (7) for the phases 1, 2, and 3, respectively, where $\dot{a}_s(t_0)$ is estimated by substituting the pressure perturbation observed in the simulations, $p_1^1(v_s t_0,t_0)$, into Eq. (2) for each phase of Fig. 2, and assuming $D=0.66$. The growth rates observed in the simulations agree very well with the theoretical values estimated from Eq. (7).

Nonlinear evolution of the instability is also investigated for the large amplitude of the rippled piston, $a_0/\lambda=0.2$ by

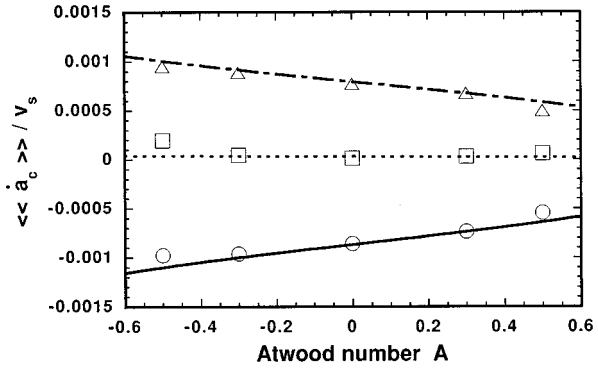

FIG. 5. Normalized asymptotic values of the growth rate, $\langle\langle \dot{a}_c \rangle\rangle / v_s$, vs Atwood number. Open circles, squares, and triangles are simulation results for the cases corresponding to phases 1, 2, and 3 in Fig. 2. The solid, dotted, and dot-dashed lines are the corresponding theoretical values.

using IMPACT-2D. The contrast in Fig. 6 indicates the isodensity contour for the Atwood number $A=-0.5$. The phases of the oscillating shock in Figs. 6(a) and 6(b) correspond to the phases 2 and 3 in Fig. 2, respectively. The black area in the top of each frame in the figures represents the rippled piston, whose surface shape is given by a sinusoid function. The first frame shows the rippled shock driven by the piston and the uniform contact surface. The second frame shows the state at the time when the shock hits the contact surface, $v_s t/\lambda = 0.7$ in Fig. 6(a) and at $v_s t/\lambda = 0.9$ in Fig. 6(b). The third and fourth frames show the transmitted shock and the unstable contact surface.

There is no asymptotic growth of the contact surface in the linear regime of phase 2. However, the mushroom shape of the contact surface appears as shown in Fig. 6(a). In the case of phase 3, the square shape of the contact surface appears as shown in Fig. 6(b). These differences between the linear and nonlinear cases are caused by the large distortion of the shock surface which is not sinusoidal any more as one can see in the first frame in Figs. 6(a) and 6(b). At phase 2 the cusplike structures appear in the shape of the shock surface at the center and both sides. The velocity impulse from the cusplike structured shock passage drives the mushroom shapes of the contact surface. Even at phase 3, the shock surface is not flat any more for the large amplitude of the rippled shock. The shock surface with little square shapes of the contact surface in Fig. 6(b). The density perturbations between the piston and contact surface in the last frames are rather complex because of the reflected rarefaction at the piston surface.

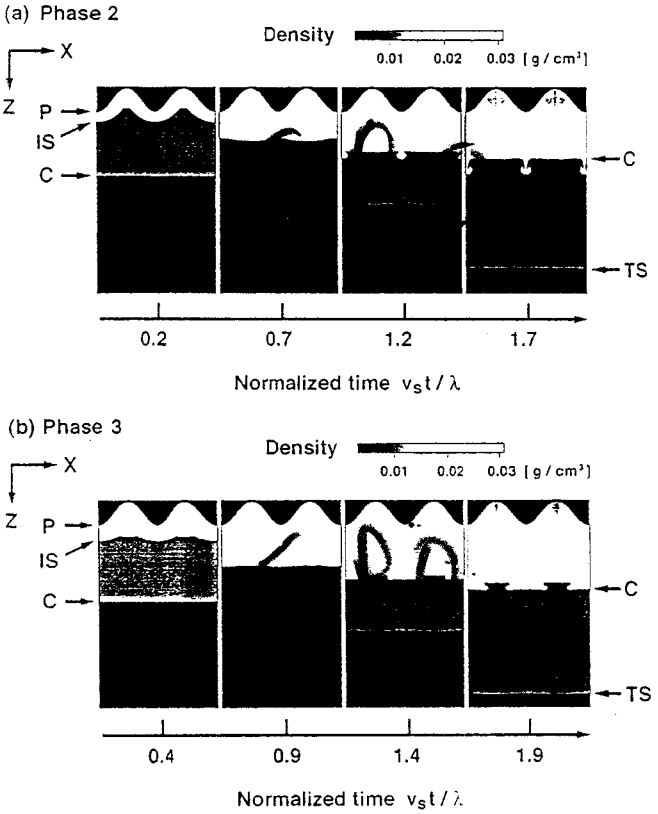

FIG. 6. Nonlinear evolutions of the instability are shown by the isodensity contours with contrast. (a) and (b) correspond to phases 2 and 3 in Fig. 2. The black area in the top of each frame in the figures represents the rippled piston. In (a) each frame corresponds to the time at $v_s t/\lambda = 0.2$, 0.7, 1.2, and 1.7, and in (b) $v_s t/\lambda = 0.4$, 0.9, 1.4, and 1.9. *P*, *C*, IS, and TS are the same as in Fig. 1.

We have found an instability of the uniform contact surface when the nonuniform shock driven by a rippled piston passes through the contact surface. Both the linear and nonlinear evolutions of the instability exhibit differences from the standard RM instability. The physical mechanism of the instability can be explained as a gravitational instability driven by the acceleration induced by the initial nonuniform shock and the pressure perturbation behind it. The growth rate depends on the phase of the oscillating shock at the time when the shock hits the contact surface.

We thank Dr. J. G. Wouchuk, Dr. M. Murakami, Professor H. Azechi, Mr. K. Shigemori, and Professor K. Mima for many useful discussions.

[1] R. D. Richtmyer, Pure Appl. Math. **13,** 297 (1960).
[2] E. E. Meshkov, Fluid Dyn. **4**, 101 (1969) [Izv. Akad. Nauk SSSR, Mekh. Zhidk. Gaza **5**, 151 (1969)].
[3] H. Sakagami and K. Nishihara, Phys. Fluids B **2**, 2715 (1990); H. Sakagami *et al.*, in *Japan U.S. Seminar on Physics of High Power Laser Matter Interactions*, edited by S. Nakai and G. H. Miley (World Scientific, Singapore, 1992), pp. 361–368.
[4] A. Harten J. Comput. Phys. **357,** 357 (1983).
[5] M. G. Briscoe and A. A. Kovitz, J. Fluid Mech. **31,** 529 (1968).
[6] G. Fraley, **29,** 376 (1986).
[7] T. Endo *et al.*, Phys. Rev. Lett. **74,** 3608 (1995).